

# Progress Towards A Measurement of Neutrino Induced Charged Current Neutral Pion Production in the MicroBooNE Experiment

The MicroBooNE Collaboration

May 25, 2022

MICROBOONE-NOTE-1107-PUB  
MICROBOONE\_INFO@fnal.gov

## Abstract

An analysis of MicroBooNE data with a signal of one muon, one neutral pion, and no charged pions is presented. Studying neutral pion production in the MicroBooNE detector provides an opportunity to better understand neutrino-argon interactions, and is crucial for future accelerator-based neutrino oscillation experiments. This analysis presents the progress towards the first measurement of the differential cross section for charged current (CC)  $\pi^0$  production in neutrino-argon interactions. Using a dataset corresponding to about  $7 \times 10^{20}$  protons on target (POT), we present an analysis which aims to measure the single differential cross sections as a function of the  $\pi^0$  kinematic variables such as momentum and scattering angle. The Wiener-SVD technique for unfolding the measurement is presented and demonstrated using multiple generator predictions. A future iteration of this analysis will compare an unfolded data measurement to these models.

# Contents

<b>1</b>	<b>Introduction</b>	<b>3</b>
<b>2</b>	<b>Signal Definition</b>	<b>3</b>
<b>3</b>	<b>Event Selection</b>	<b>3</b>
<b>4</b>	<b>Systematic Uncertainty</b>	<b>5</b>
<b>5</b>	<b>Data Simulation Comparison of the Kinematic Variables</b>	<b>7</b>
<b>6</b>	<b>Cross section Extraction</b>	<b>9</b>
<b>7</b>	<b>Conclusion</b>	<b>11</b>

# 1 Introduction

The analysis reported in this note outlines progress towards the first differential measurement of neutrino induced charged current (CC) neutral pion production in the MicroBooNE Experiment [1]. The event topology for this measurement contains a muon, a single  $\pi^0$ , any number of nucleons, and no charged pions in the final state. The charged current interaction of a muon neutrino producing a single neutral pion most commonly occurs through the  $\Delta$  resonance for neutrinos with energy below 2 GeV. There is no coherent contribution possible in this process since the final state for CC coherent pion production includes a charged pion. Lack of a coherent contribution makes this process an ideal probe of incoherent processes and thus helps us understand the pion production mechanism along with other phenomenological effects.

The work described in the following sections builds on a previous MicroBooNE study. The current measurement is based on the Pandora reconstruction framework.

This report focuses on a detailed description of progress towards a measurement of the differential cross section as a function of the outgoing  $\pi^0$  momentum and the scattering angle with respect to the beam direction.

## 2 Signal Definition

A neutrino scattering event is chosen as part of the signal if it satisfies the following requirements:

- The final state contains one muon with kinetic energy greater than 20 MeV.
- The final state contains exactly one neutral pion
- The final state contains zero charged pions with kinetic energy greater than 40 MeV.
- No requirement on the number of nucleons

The specific requirements on the neutral pion are described in this section. The above signal definition is consistent with recent measurements reported by the MiniBooNE experiment in 2011 [2] and the MINERvA experiment in 2015 [3] on a carbon target, and hence enables us to study the effect of the change of the nuclear target and allows for a direct comparison across experiments.

## 3 Event Selection

The signature for this analysis comes from  $\nu_\mu$  CC interactions within the fiducial volume, and consists of a muon track, a  $\pi^0$ , and any number of nucleons while vetoing on tracks identified as  $\pi^\pm$ . The event selection focuses on identifying muon neutrino induced  $\pi^0$  in a CC interaction where the  $\pi^0$  decays to photons, which each then pair-produce  $e^+e^-$ . The pair-production of photons dominates over Compton scattering for the MicroBooNE energy range. Hence, the event selection focuses on looking for  $\nu_\mu$  CC events associated with two photon showers from the  $\pi^0$ , a muon track, any number of nucleons, and no charged pions. Neutrino events are reconstructed in this analysis using the Pandora pattern recognition toolkit[4].

Before diving into the major steps of event selection, we look at a low-level identification of a neutrino induced event as well as the containment and cosmic-rejection requirements. A large fraction of backgrounds coming from cosmic induced, out-of-cryostat, and out-of-TPC active volume events are removed by requiring the neutrino interaction vertex to be contained within a fiducial volume (FV). The dimensions of the FV in this analysis are,  $3.45 \text{ cm} \leq x \leq 249.8 \text{ cm}$ ,  $-109.53 \text{ cm} \leq y \leq 111.47 \text{ cm}$ ,  $20.1 \text{ cm} \leq z \leq 986.9 \text{ cm}$ . The x axis is along the negative drift direction with 0 at the anode plane, y is vertically upward with 0 at the center of the detector, and z is along the beam direction, with 0 at the upstream edge of the detector. Additionally, the contained fraction variable, defined as the ratio of number of hits contained in the FV to the total hits clustered in the neutrino slice, is required to be  $> 0.4$ . Due to the near surface location of the MicroBooNE detector, it observes a large amount of cosmic induced events, the beam-off backgrounds are relatively large near the top of the TPC (high values of y-coordinate) due to cosmics entering from above. The topological score, a variable designed to distinguish neutrino induced events from cosmic-like events, is set to  $> 0.1$ . The cosmic impact parameter is defined

as the shortest distance between the shower start point and any reconstructed hit tagged by Pandora as cosmic-induced. We require the 3D cosmic impact parameter to be  $> 30$  cm in order to further reject cosmic background. To remove neutrino induced backgrounds, we leverage Pandora's track/shower classification, encoded as a single variable in which values closer to 1 are classified as track-like, and values closer to 0 as shower-like. We require the leading shower score to be  $< 0.25$ .

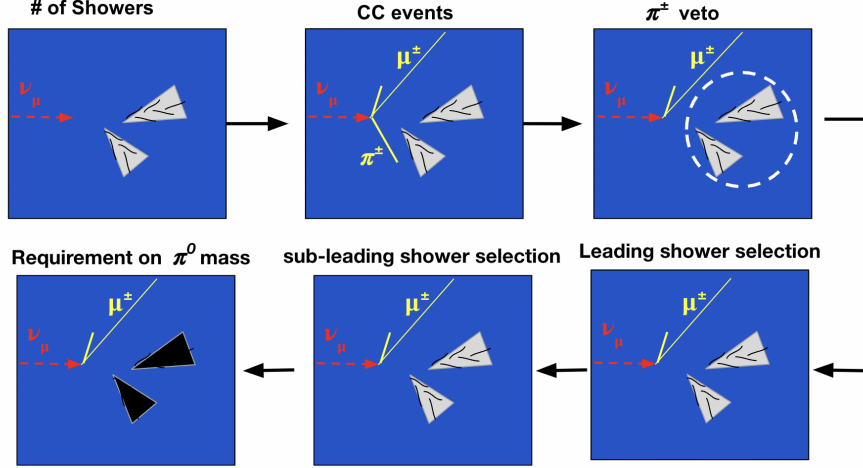


Figure 1: Visual representation of the major steps of event selection

The major selection steps are listed below, and shown in Fig(1):

- **Shower requirement** : We select events with 2 or 3 Pandora-reconstructed showers as the  $\pi^0$  decays predominantly to two photon electromagnetic showers.
- **CC inclusive selection** : A muon candidate is selected based on the longest track with a suitable particle identification (PID) score that also satisfies quality requirements. The PID used is described in more detail in ([5]).
- **Charged pion veto** : The veto is implemented by constraining the number of MIP-like tracks to only one. The MIP-like track is selected by requiring the PID score on the longest track to be greater than 0.6 and the track-score variable to be greater than 0.5.
- **Leading shower requirement** : Events that have a leading shower with the radial angle within 0.45 radians (cosine angle  $> 0.9$ ) are selected. We select events with  $2 \text{ cm} < \text{conversion distance} < 80 \text{ cm}$  OR  $dE/dx > 2.5 \text{ MeV/cm}$  for events with conversion distance  $< 2 \text{ cm}$ . Fig.(2) shows an illustration of the conversion distance and the radial angle. The conversion distance refers to the distance between the Pandora event vertex and the shower start point. The radial angle is the angle between the shower axis and the vector between the vertex and the shower start point.
- **Sub-leading shower requirement** : Events with a sub-leading shower energy  $> 10 \text{ MeV}$ , and a conversion distance  $> 1 \text{ cm}$  OR  $dE/dx > 2.5 \text{ MeV/cm}$  for showers with conversion distance  $< 1 \text{ cm}$ . In events with three Pandora-reconstructed showers, only the second-highest energy shower is considered as a sub-leading shower candidate. The lowest-energy shower is not considered.
- **Reconstructed  $\pi^0$  mass** : To further constrain the showers, we require the reconstructed  $\pi^0$  mass to be within  $[50, 180] \text{ MeV}$ .

The final signal selection efficiency is 7.5% and the purity is 70%.

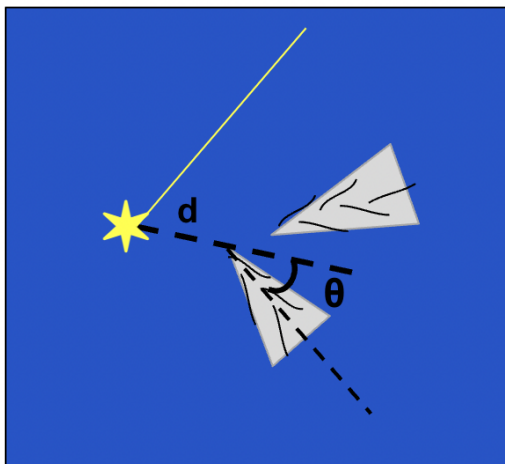


Figure 2: The conversion distance,  $d$  and the radial angle  $\theta$  are shown in the illustration.

## 4 Systematic Uncertainty

The systematic uncertainties for this measurement come from the Booster Neutrino Beam (BNB) flux, neutrino interaction modeling, reinteraction modeling, and variation of detector simulation parameters. As the differential cross-section is measured across multiple bins that are correlated, we evaluate the covariance matrix.

The total covariance matrix encodes the statistical and systematic uncertainties [6].

$$V = V_{\text{sys}} + V_{\text{stat}} \quad (1)$$

where  $V_{\text{sys}}$  is the sum of all covariance matrices from all of the contributions discussed in the next section, and  $V_{\text{stat}}$  consists of an uncorrelated diagonal statistical covariance. The covariance matrix is calculated following MicroBooNE's multiple universe procedure. The major sources of the systematic uncertainties are the following:

- Interaction model uncertainties : The systematic uncertainties on the interaction model incorporate uncertainties on the MicroBooNE GENIE tune and are described in ([7]).
- Flux uncertainties : The flux uncertainties are split into two categories, those arising from hadron production modelling and the beamline geometry, with the former dominating.
- Re-interaction : The outgoing particles from the primary neutrino interaction may re-interact with other nuclei inside the detector.
- Detector Effects : The uncertainties are estimated by simulating a set of neutrino interactions in the MicroBooNE detector, which are fed into several detector models. These sets of events are reconstructed and fed through the selection. The difference between the number of events selected using the default detector model and an alternative model is used as an uncertainty.

Figs.(3-4) show the fractional uncertainties on the number of reconstructed events in each bin estimated by employing procedures described in the previous sub-sections for the outgoing  $\pi^0$  momentum and the cosine angle. The total uncertainty is shown by a dashed black line. For some of the momentum and the angular bins, the detector uncertainties dominate. In some of the bins uncertainties arising from flux and GENIE modeling are higher. Re-interaction uncertainties are small and relatively flat across all bins.

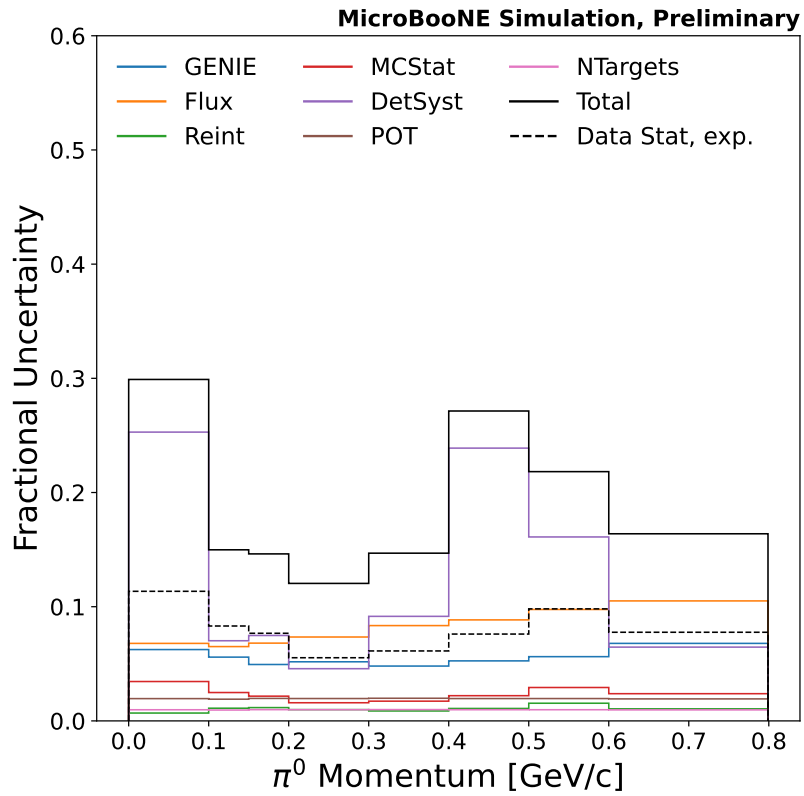


Figure 3: Summary of the total fractional uncertainty coming from GENIE, Flux, Re-interaction and detector variations for the  $\pi^0$  momentum.

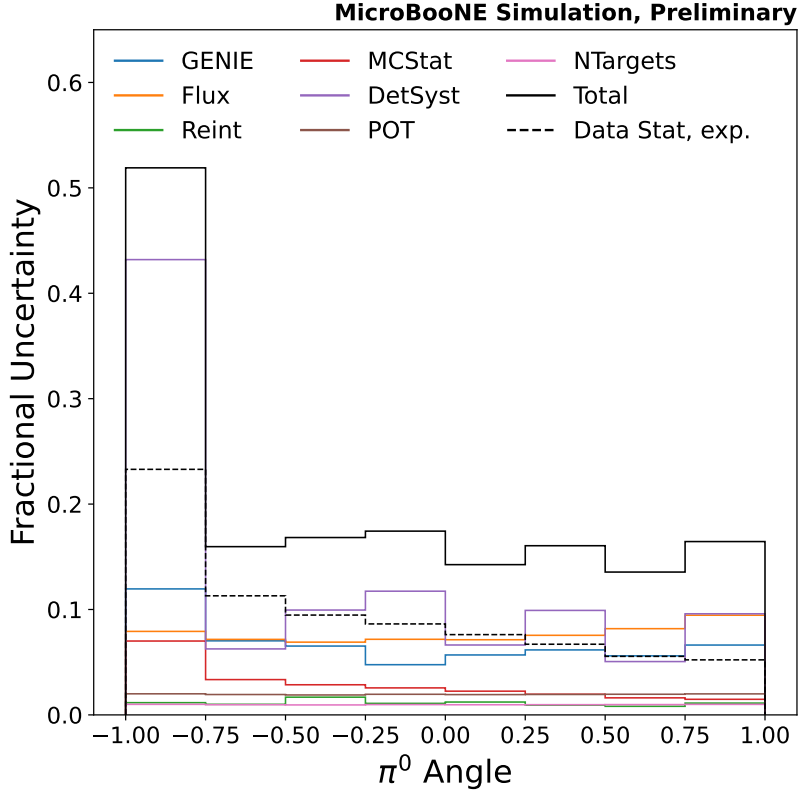


Figure 4: Summary of the total fractional uncertainty coming from GENIE, Flux, Re-interaction and detector variations for the  $\pi^0$  cosine angle.

## 5 Data Simulation Comparison of the Kinematic Variables

The observed distribution for the kinematic variables considered in this analysis are shown in Figs.(5-6), showing the comparison between data and overall prediction for all selected events. In this analysis the nominal simulation is based on the tuned version of GENIE v3 ([7]). For both distributions, data agrees with the overall predictions within the total uncertainties. The shaded error-bands in Figs.(5-6) include Monte Carlo (MC) simulation statistical errors, flux, cross-section, re-interaction uncertainties, and detector systematics. EXT and BNB refer refer to data collected when the BNB beam was off, and when the BNB beam was on respectively in the plots.

Run 123 - 2+ showers - Pi0 Presel.  
 CC pi0 selection - No pi0 Scaling

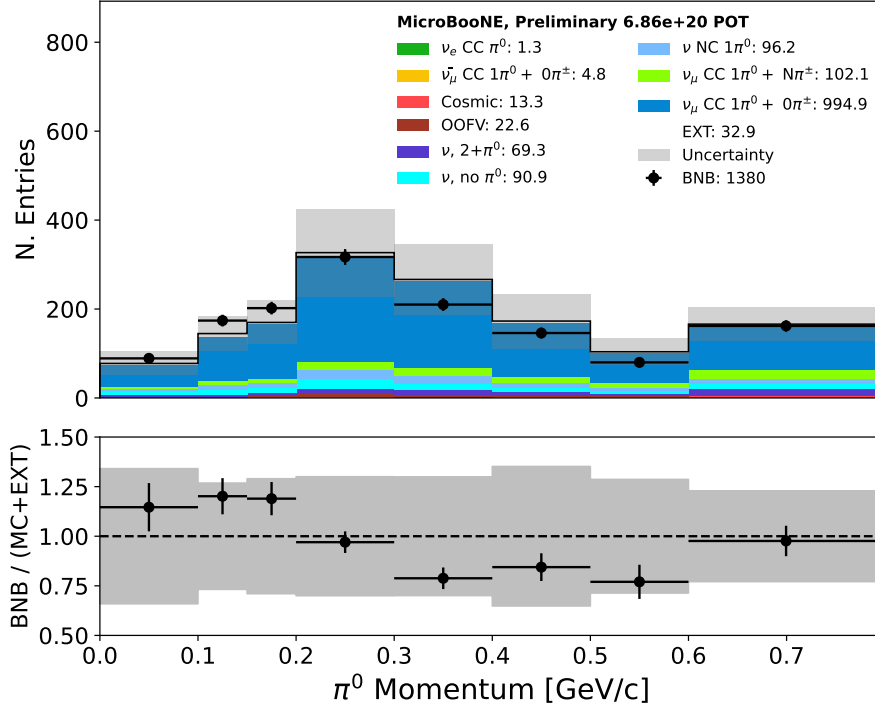


Figure 5: Momentum of the  $\pi^0$  shown in the bins for which the differential cross-section will be estimated. The shaded error bands include MC statistical errors, flux, cross-section, re-interaction, and detector uncertainties.



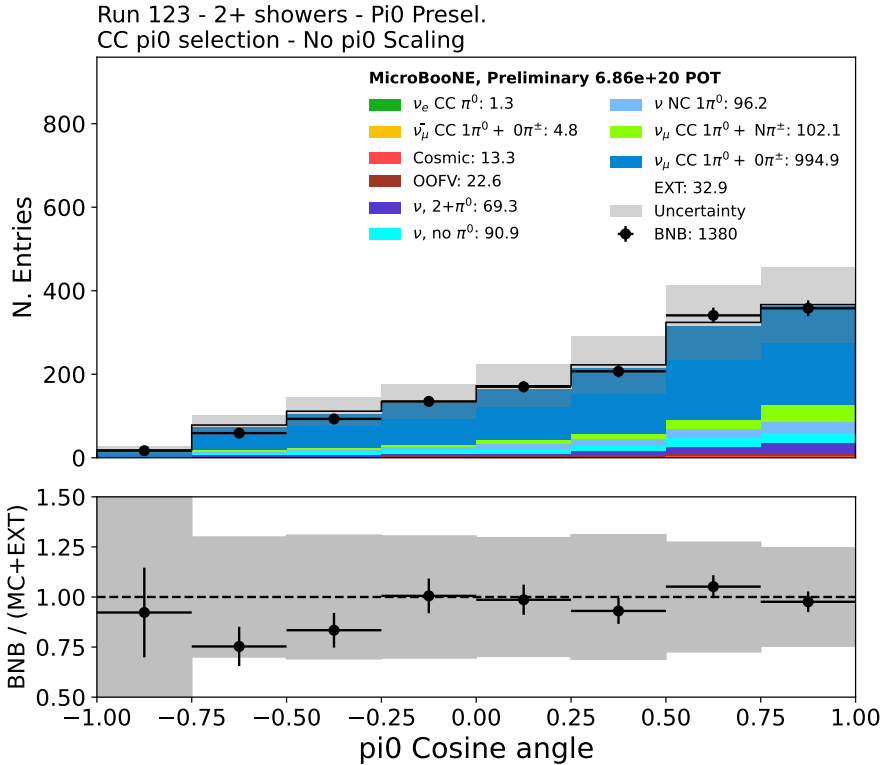


Figure 6: Cosine angle of the  $\pi^0$  shown in the bins for which the differential cross-section will be estimated. The angle is defined as the direction of  $\pi^0$  with respect to the beam direction. The shaded error bands include MC simulation statistical errors, flux, cross-section, re-interaction, and detector uncertainties.

## 6 Cross section Extraction

This section focuses on the methodology of extracting the differential cross-section as a function of the outgoing  $\pi^0$  kinematic variables. The  $\pi^0$  kinematic variables studied in this note are sensitive to the underlying interaction as well as final state interactions. This analysis presents the progress towards the first measurement of the differential cross section for  $\pi^0$  production in neutrino-argon interactions. The differential cross-section is given by

$$\left\langle \frac{d\sigma}{dp} \right\rangle_i = \frac{\sum_j U_{ij}(N_j - B_j)}{N_{\text{target}} \times \phi \times (\Delta p)_i} \quad (2)$$

where the unfolding matrix elements  $U_{ij}$  transforms the background subtracted reconstructed events in a given bin  $j$  to true bin  $i$ , and  $(\Delta p)_i$  is the width of bin  $i$ .  $N_j$ , and  $B_j$  are the number of selected data events and background events respectively in bin  $j$ .  $\phi$  and  $N_{\text{target}}$  correspond to the flux and the number of argon targets in the fiducial volume.

The cross-section results in this note will be extracted after unfolding in true space using the Wiener-SVD unfolding method. An unfolded result can be directly compared to various generator predictions as it removes the detector effects from the measurement. The unfolding method requires an inversion of the response matrix that potentially leads to an unfolded distribution with amplified statistical and systematic uncertainties, and hence leading to a large variance in the truth space. To account for such an effect, regularization or smoothness conditions are applied. Regularization inevitably introduces a bias but allows for easier interpretations. Further details about the Wiener-SVD method can be found in ([8]). The background-subtracted data, the covariance matrix accounting for the systematic and the statistical uncertainties, and the response matrix are the inputs for this method. It returns an unfolded signal distribution in a smeared true space as well as the unfolded covariance matrix and an additional smearing matrix. The smearing matrix along with the true signal event distribution provides a smeared true model prediction that

can then be compared to the unfolded data. The unfolding framework used in this analysis is developed internally by MicroBooNE collaborators.

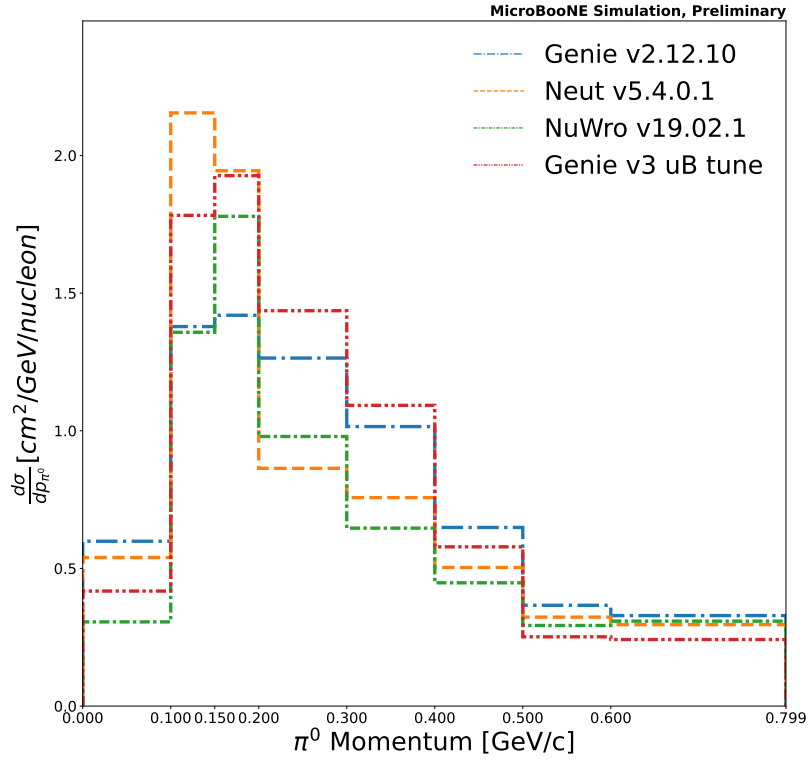


Figure 7: Generator prediction comparisons for  $\pi^0$  momentum

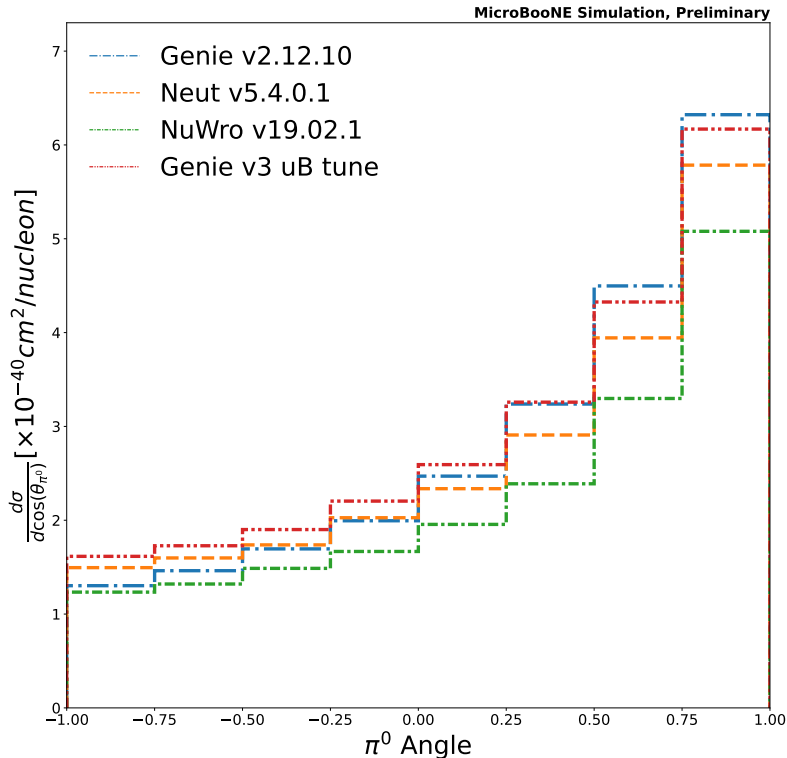


Figure 8: Generator prediction comparisons for the cosine angle of  $\pi^0$

Figs 7 and 8 show the comparisons from different generator predictions for the pion kinematic variables. Qualitative differences between predictions are observed in analysis variables and binning. We will validate the cross-section results extracted from MicroBooNE data with various neutrino generators such as NEUT v5.4.01 [9], NuWro v19.02.1 [10], GENIE v2.12.10 [11][12]. Details about the models used in these generators and a more complete description of their differences can be found in other MicroBooNE publications [13],[14].

## 7 Conclusion

The methodology used to estimate the differential cross section has been described in this note. This includes the stages of event selection, calculation of systematic uncertainties and cross section extraction procedure. The measurement presented in this note corresponds to  $6.86 \times 10^{20}$  POT from the BNB beam. The final cross section data results in pion and muon kinematic variables will be presented in near future.

## References

- [1] R. Acciarri et al. (MicroBooNE Collaboration), “Design and construction of the MicroBooNE detector”, *Journal of Instrumentation* **12**, P02017–P02017 (2017).
- [2] A. A. Aguilar-Arevalo et al. (MiniBooNE Collaboration), “Measurement of  $\nu_\mu$ -induced charged-current neutral pion production cross sections on mineral oil at  $E_\nu \in 0.5 - 2.0$  GeV”, *Phys. Rev. D* **83**, 052009 (2011).
- [3] O. Altinok et al. (MINERvA Collaboration), “Measurement of charged-current single  $\pi^0$  production on hydrocarbon in the few-gev region using minerva”, *Physical Review D* **96**, 10.1103/physrevd.96.072003 (2017).

- [4] P. Abratenko et al. (MicroBooNE Collaboration), *The European Physical Journal C* **78**, [10.1140/epjc/s10052-017-5481-6](https://doi.org/10.1140/epjc/s10052-017-5481-6) (2018).
- [5] P. Abratenko et al. (MicroBooNE Collaboration), “Calorimetric classification of track-like signatures in liquid argon TPCs using MicroBooNE data”, *Journal of High Energy Physics* **2021**, [10.1007/jhep12\(2021\)153](https://doi.org/10.1007/jhep12(2021)153) (2021).
- [6] P. Abratenko et al. (MicroBooNE Collaboration), <https://microboone.fnal.gov/wp-content/uploads/MICROBOONE-NOTE-1099-PUB.pdf>.
- [7] P. Abratenko et al. (MicroBooNE Collaboration), “New genie model tune for MicroBooNE”, *Physical Review D* **105**, [10.1103/physrevd.105.072001](https://doi.org/10.1103/physrevd.105.072001) (2022).
- [8] W. Tang, X. Li, X. Qian, H. Wei, and C. Zhang, “Data Unfolding with Wiener-SVD Method”, *JINST* **12**, P10002 (2017).
- [9] Y. Hayato and L. Pickering, “The NEUT neutrino interaction simulation program library”, *The European Physical Journal Special Topics* **230**, 4469–4481 (2021).
- [10] T. Golan, C. Juszczak, and J. T. Sobczyk, “Effects of final-state interactions in neutrino-nucleus interactions”, *Physical Review C* **86**, [10.1103/physrevc.86.015505](https://doi.org/10.1103/physrevc.86.015505) (2012).
- [11] C. Andreopoulos et al., “The GENIE neutrino monte carlo generator”, *Nucl. Instrum. Meth. A* **614**, 87–104 (2010).
- [12] C. Andreopoulos et al., “The genie neutrino monte carlo generator: physics and user manual”, [arXiv:1510.05494](https://arxiv.org/abs/1510.05494), [10.48550/ARXIV.1510.05494](https://doi.org/10.48550/ARXIV.1510.05494) (2015).
- [13] P. Abratenko et al. (MicroBooNE Collaboration), “First measurement of differential charged current quasielasticlike  $\nu_\mu$ -argon scattering cross sections with the microboone detector”, *Phys. Rev. Lett.* **125**, 201803 (2020).
- [14] P. Abratenko et al. (MicroBooNE Collaboration), “Measurement of differential cross sections for  $\nu_\mu$ -ar charged-current interactions with protons and no pions in the final state with the microboone detector”, *Phys. Rev. D* **102**, 112013 (2020).